Dynamics of Polarization Switching in Mixed Phase Ferroelectric-Antiferroelectric HZO Thin Films

Hannes Dahlberg
Department of Electrical and Information Technology, Lund University
Division of Electromagnetics and Nanoelectronics
Lund, Sweden
hannes.dahlberg@eit.lth.se

Lars-Erik Wernersson
Department of Electrical and Information Technology, Lund University
Division of Electromagnetics and Nanoelectronics
Lund, Sweden
lars-erik.wernersson@eit.lth.se

***Abstract*—The polarization switching dynamics for $Hf_{1-x}Zr_xO_2$ (HZO) integrated on InAs is studied as a function of pulse width and amplitude. Due to a mixed ferroelectric/antiferroelectric phase at x=0.8, a more gradual total polarization update is shown compared to a fully ferroelectric $Hf_{0.5}Zr_{0.5}O_2$ stack. A lowered operating voltage is achieved in $Hf_{0.2}Zr_{0.8}O_2$ by activating an inner ferroelectric hysteresis loop, and the switching dynamics of this inner hysteresis is studied. The Nucleation-Limited Switching (NLS) model is used to determine switching times for both stacks and show increased switching speeds for low-voltage polarization in the $Hf_{0.2}Zr_{0.8}O_2$ inner hysteresis, suggesting a benefit of using high-Zr HZO for higher speed and lower operating voltages.**

***Index Terms*—ferroelectricity, HZO, antiferroelectricity, polarization, switching dynamics, Indium Arsenide**

I. Introduction

Ferroelectric (FE) $Hf_{1-x}Zr_xO_2$ (HZO) thin films have displayed a large potential for future non-volatile memories, especially for ultra-low energy operations and neuromorphic computing [1]. Ferroelectric field-effect transistors (FeFET), tunnel junctions (FTJ) and random-access memory (FeRAM) are all devices based on the non-volatile ferroelectric polarization for either modulation of device current or as a state to be read and written [2]. HZO as a material is attractive for these applications as it is very scalable and compatible with modern Si-based nodes and back-end-of-line (BEOL) integration [3]. By increasing the Zr concentration in $Hf_{1-x}Zr_xO_2$, a transition to antiferroelectric (AFE) behavior can be observed [4]. As a design consideration, a higher Zr concentration shows benefits such as higher permittivity and lower crystallization temperature [4]–[6]. AFE-based memory devices have also been reported to benefit from lower operating voltages, lower switching stress and better endurance, making Zr-rich HZO devices highly relevant for further device research [6]–[8].

The dynamics of polarization switching is essential, as it sets a constraint on the read and write-schemes used in the system. This has been studied for fully FE devices, and to some degree for AFE devices, but is less characterized for FE/AFE mixed phase devices [9]–[11]. The FE-AFE transition of $Hf_{1-x}Zr_xO_2$ integrated on indium arsenide (InAs) shows that high-Zr (80%) HZO-based metal-ferro-semiconductor (MFS) capacitor display a relatively large remanent polarization (P_r) compared to classic TiN-based metal-ferro-metal (MFM) devices at identical Zr concentrations [12]. Due to this fact, an inner FE hysteresis can be accessed, with a reduced coercive field (E_C), enabling lower-voltage operations while still displaying a polarization usable for non-volatile memory devices. It is also of interest to study the switching dynamics as results of the nucleation-limited switching (NLS) model, where the FE film is assumed to consist of different domains with a distribution of independent switching times.

In this paper, we study and compare the switching dynamics of $Hf_{0.2}Zr_{0.8}O_2$ and $Hf_{0.5}Zr_{0.5}O_2$ integrated on InAs and evaluate the experimental data with the NLS model. The inner FE hysteresis for $Hf_{0.2}Zr_{0.8}O_2$ is shown to have switching dynamics coherent with the NLS theory, and faster extracted switching speeds compared to $Hf_{0.5}Zr_{0.5}O_2$, illustrating the benefit of using high-Zr HZO for fast non-volatile operations.

II. Device Fabrication and Experimental Setup

The processing of the devices is summarized in Fig. 1 (a) and described further in [12]. An Al_2O_3 layer ($\approx$ 1.2 nm) is deposited by thermal atomic-layer deposition (ALD) directly on low-doped (n-type, 1.7e16 cm^{-3}) InAs substrate acting as the bottom electrode (BE), followed by $\approx$ 10 nm $Hf_{1-x}Zr_xO_2$. For $Hf_{0.5}Zr_{0.5}O_2$, the Hf-Zr oxide layers are grown 1:1 (referred to as 50% Zr). For $Hf_{0.2}Zr_{0.8}O_2$, the Hf-Zr oxide is instead grown 1:4 (referred to as 80% Zr). TiN is used as top electrode (TE) and the devices are annealed at 550 ^{o}C for 30 s. This forms a metal-ferro-insulator-semiconductor (MFIS) capacitor which is then defined in area as circular devices with a radius of 15 μm (Fig. 1 (b)).

Electrical characterization is performed in a CRX-6.5K probe station with a Keysight B1500 semiconductor analyzer and B1530A waveform generators. The measurement setup is illustrated in Fig. 1 (b). 1000 square-wave pulses (1 kHz) at $\pm$3 V is used as wake-up for all devices before measuring. Bipolar pulsing for polarization hysteresis measurements is performed with 10 kHz triangular pulses. A device area = $\pi \cdot 15^2$ μm^2, relative permittivity $\approx$ 25 (from [12]) and measured probe

This work was supported in part by the MISEL project (EU Horizon 2020, Grant 101016734) and the European Research Council Grant 101019147.

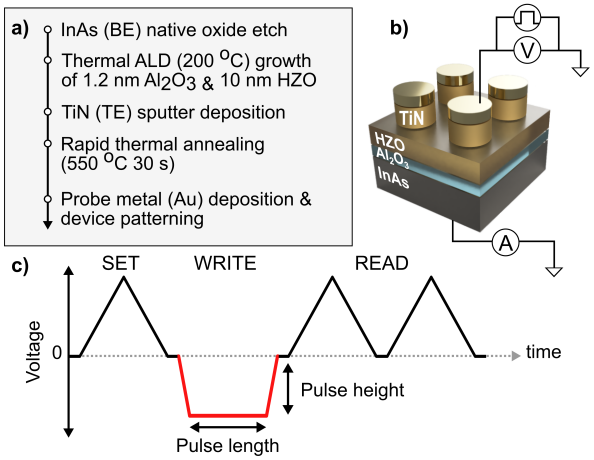

Fig. 1. Summary of the MFIS process flow (a). Measurement setup using B1530A waveform generators and schematic of MFIS stack (not to scale) (b). Pulse scheme for measuring polarization of a pulse with certain pulse length and height, with a SET pulse and subsequent READ pulses of identical polaritites (c).

series resistance $\approx 40\ \Omega$ gives the measurement setup an RC time constant of approximately 0.6 ns.

When measuring switching dynamics, the polarization switching is analyzed as a function of a WRITE pulse width and amplitude. Due to limitations in current measurement at ultra-short pulses, it is necessary to read the WRITE pulse polarization with a re-polarizing measurement (illustrated in Fig. 1 (c)). The polarization is first SET with a 80 μs triangular pulse. A WRITE pulse with varying length and height and a 10 ns rise-and fall time is then applied with the opposite polarity to the end SET pulse. This is followed by two READ pulses of the same polarity as the SET pulse (80 μs each). The corresponding polarization switching from the WRITE pulse is then expected to be re-switched with the READ pulse. The second READ pulse can be used to remove the contribution from volatile switching and/or the leakage contribution. Before and after the WRITE pulse there is a 10 μs delay.

III. Experimental Results

The Polarization-Voltage (P-V) hysteresis for 50% Zr and 80% Zr is shown in Fig. 2 (a-b), with the corresponding Current-Voltage response in Fig. 2 (c-d). 80% Zr exhibits a mixed FE/AFE hysteresis, as there exists a P_r at zero fields. Both hysteresis curves are shifted toward positive biases from the internal field equal to the flat band voltage between InAs and TiN [12]. As can be seen in Fig. 2 (b), an inner FE loop is accessible for 80% Zr with lower bias fields. This avoids the switching at high positive biases (and the following back-switching, labeled as **I** and **I*** respectively in Fig. 2 (d)), instead only accessing the switching and back-switching from the negative side of the hysteresis (**II** and **II***). Due to the internal field discussed above, this switching and back-switching are somewhat separated on different sides of 0 V, creating a FE-like switching for low fields.

In Fig. 3, the dynamic pulse-scheme in Fig. 1 (c) is applied to woken-up 50% Zr and 80% Zr samples, for -3.5 V SET/READ and positive WRITE (top figure), as well as for +3.5 V SET/READ and negative WRITE (bottom figure). The switching dynamics for 50% Zr in Fig 3 (a) display a polarization update consistent with previous work as well as that stated by the NLS model (discussed further in section IV) [9], where the polarization saturates for larger voltages at a certain pulse width. 80% Zr, however, shows little saturation in the polarization update for large amplitudes and pulse widths, but instead a gradual increase in polarization when the AFE-like back-switching is present. The gradual increase in $2P_r$ suggests that the back-switching does not fully cancel the FE switching. This can be seen in Fig. 2 (b), where the measured inner FE hysteresis is not fully extended to the edge of the total hysteresis at zero biases. The internal field hysteresis-shift discussed above is also seen as asymmetric polarization switching for both 50% and 80% Zr devices.

There is a gap between zero polarization and the measured values in the "negative WRITE" case in Fig. 3 (b). This can be understood by observing the inner FE hysteresis in Fig. 2 (b), which looks more saturated for positive biases compared to negative. This is due to the inner FE loop originating from the offset negative bias switching and AFE-like back-switching. Thus, for +3.5 V READ pulses (negative WRITE pulses) the positive-bias AFE switching/back-switching (**I / I*** in Fig. 2 (d)) will be accessed and seen as an always-present polarization in the READ pulse.

In Fig. 3 (b), the 80% Zr switching dynamics at polarization up to $\pm 20\ \mu$C/cm^2 (marked in Fig. 3 (b) as "Inner FE") is shaped like that of the full pulse range of 50% Zr (disregarding

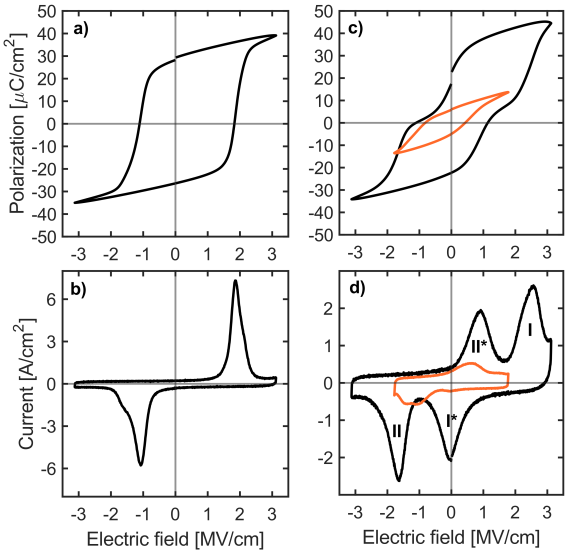

Fig. 2. Polarization-Voltage hysteresis of $Hf_{0.5}Zr_{0.5}O_2$ MFIS devices (a, b) and $Hf_{0.2}Zr_{0.8}O_2$ MFIS devices, with inner FE loops in 80% Zr devices with switching/backswitching current pairs labeled as **I / I*** and **II / II*** (c, d). The full hysteresis switching is performed with ± 3.5 V, the inner FE loop switching in (c, d) with ± 2 V.

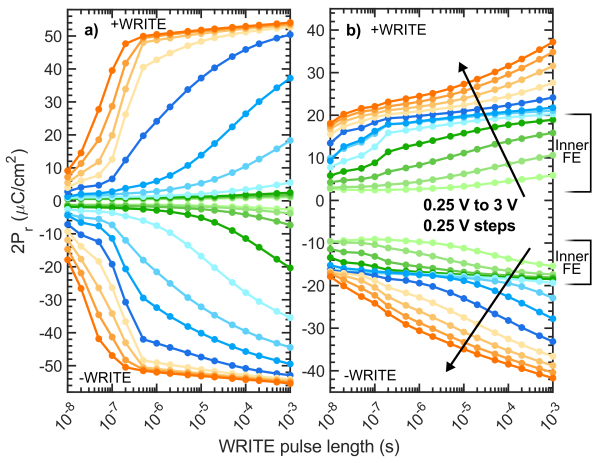

Fig. 3. Switching dynamics for 50% Zr (a) and 80% Zr (b). The re-polarization from the first READ pulse is shown as a function of WRITE pulse length for varying WRITE amplitudes, with the WRITE polarity corresponding to the polarization polarity. The WRITE pulse voltage is varied from ±0.25 V to ±3 V, with ±0.25 V steps (indicated by the arrows). The SET/READ voltages are ∓ 3.5 V. In (b), the FE-like inner-loop switching dynamics are highlighted.

the AFE contribution and polarization range difference). This illustrates the dynamic switching of a fully inner FE loop hysteresis. The continued polarization update of more gradual character could potentially benefit operations in analog computing using gradually set analog weights, where robust control of the polarization would be important [13].

IV. Modelling Methods and Results

The NLS model has proven an accurate description for the ferroelectric polarization dynamics, where the polarization switches as an ensemble of many individual regions that switches independently with a field-dependent switching time and has been validated experimentally for Hf-based ferroelectric thin films [9], [14]. The polarization update is modelled as [14]:

$$\Delta P = 2P_{\mathrm{r,\,max}} \int_{-\infty}^{\infty} \left(1 - \exp\left[-\left(\frac{t_{\mathrm{d}}}{t_{\mathrm{sw}}}\right)^2\right]\right) \cdot F(\log t_{\mathrm{sw}})\, d(\log t_{\mathrm{sw}}) \qquad (1)$$

Where ΔP is the polarization update, $P_{\mathrm{r,\,max}}$ the maximum remanent polarization, t_{d} the WRITE pulse width. $F(\log(t_{\mathrm{sw}}))$ is a Lorentzian distribution of the logarithmic switching time as

$$F(\log t_{\mathrm{sw}}) = \frac{1}{\pi}\left(\frac{\omega}{(\log t_{\mathrm{sw}} - \log t_{\mathrm{mean}})^2 + \omega^2}\right) \qquad (2)$$

Where ω and $\log(t_{\mathrm{mean}})$ are the width and center of the distribution.

The purely FE polarization update (50% Zr) is used to fit the NLS model from (1) and (2) in Fig. 4 (a) with good agreement. As discussed, 80% Zr exhibits an inner FE loop with a lowered E_{C}, observable in Fig. 2 (b) and the switching dynamics in Fig. 3 (b) up to a certain polarization. This "Inner FE" region is modeled using NLS in Fig. 4 (b), with the AFE contribution present in the second READ pulse subtracted, up to this polarization (20 μ/cm^2 for positive WRITE and -11 μ/cm^2 for negative WRITE). The resulting polarization update is coherent to the NLS model for both negative and positive WRITE pulses and illustrates the inner FE hysteresis operations as a similar one to a fully FE hysteresis in a 50% Zr stack. The non-volatile polarization continues to increase as we access more of the inner FE hysteresis switching, but with increasing AFE-like back-switching as we do so with WRITE dynamics that access the entirety of the hysteresis.

The following empirical relationship between the field-dependent switching time t_{mean} and applied voltage can be made:

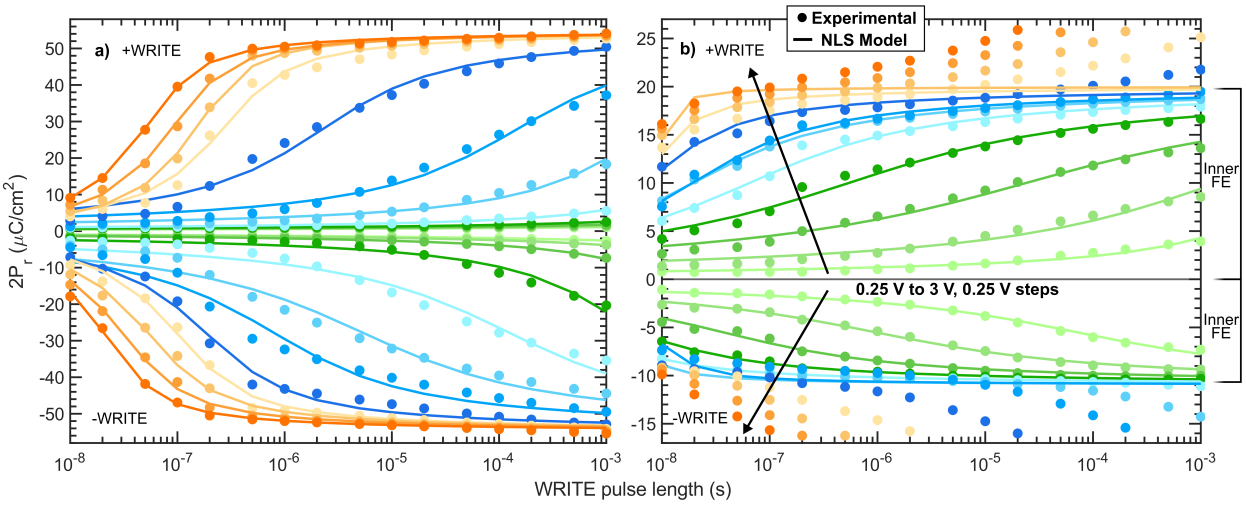

Fig. 4. Nucleation-Limited Switching modeling of switching dynamics for 50% Zr (a) and 80% Zr (b). In (b), the AFE contribution from the READ pulse is removed by subtraction from the consecutive READ pulse. The fit in (b) is limited to abs($2P_{\mathrm{r,\,max}}$) = 20 μm/cm^2 and -11 μm/cm^2 for positive and negative WRITE respectively. The arrow indicates the increase of WRITE pulse voltage from ±0.25 V to ±3 V, with ±0.25 V steps.

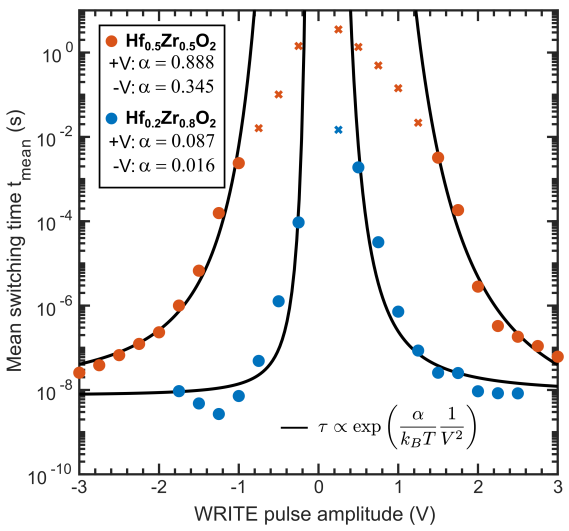

Fig. 5. Mean switching time t_{mean} for a different WRITE pulse voltages for 50% Zr and 80% Zr. The experimental results are fitted with (3). Data points excluded from the fit are marked as "x" (observe that all voltages below -1.75 V (-WRITE) and above 2.5 V (+WRITE) are excluded for 80% Zr).

$$\tau \propto \exp\left(\frac{\alpha}{k_B T}\frac{1}{V^2}\right) \tag{3}$$

where α is a fitting parameter coupled to intrinsic material properties such as domain wall energy, k_B is Boltzmann's constant, and T is the temperature [15]. Using (3) and the mean switching times determined from the NLS fit (excluding switching times for near non-switching and instantly switching pulse amplitudes) in Fig. 4, the relationship between switching time and WRITE voltage is fitted and can be seen in Fig. 5. The fit between (3) and the experimental data further shows the agreement between the NLS model and the measurements, both for 50% and 80% Zr. 80% Zr devices displays shorter mean switching times for the inner FE hysteresis polarization compared to 50% Zr. A reduction of α (Fig. 5 inset) for the higher Zr devices further indicates a lowered switching barrier energy. This together with a lowered E_C could enable faster domain switching for the dipole switching in the material, compared to 50% Zr which need larger and more separated bias fields for switching [16]. Note that in Fig. 4 (b), the negative WRITE dynamics show an almost full polarization already at the shortest WRITE pulse (10 ns) larger than -1 V. The mean switching times for these voltages are difficult to accurately determine, so the fit of (3) to these points in Fig. 5 should be regarded with this in mind. Nonetheless, the trend is still clear.

V. Conclusions

The polarization switching dynamics for a FE/AFE-mixed HZO ($Hf_{0.2}Zr_{0.8}O_2$) thin film on InAs have been measured and compared to a purely FE device ($Hf_{0.5}Zr_{0.5}O_2$). The NLS model is fitted to the experimental data and used to determine the mean switching time. 80% Zr devices displayed a faster switching of its non-volatile inner FE loop compared to 50% Zr devices, due to the lowered E_C for the inner non-volatile switching and a lowered intrinsic switching barrier energy. Switching speed and operating voltage are both important parameters for future low-energy memory devices, thus motivating the use of Zr-rich HZO.

References

[1] M. H. Park, Y. H. Lee, T. Mikolajick, U. Schroeder, and C. S. Hwang, "Review and perspective on ferroelectric HfO2-based thin films for memory applications," MRS Commun, vol. 8, no. 3, pp. 795–808, Sep. 2018, doi: 10.1557/mrc.2018.175.

[2] T. Mikolajick et al., "Next generation ferroelectric materials for semiconductor process integration and their applications," J Appl Phys, vol. 129, no. 10, p. 100901, Mar. 2021, doi: 10.1063/5.0037617.

[3] H. Mulaosmanovic, E. T. Breyer, S. Dünkel, S. Beyer, T. Mikolajick, and S. Slesazeck, "Ferroelectric field-effect transistors based on HfO2: a review, "Nanotechnology, vol. 32, no. 50, p. 502002, Dec. 2021, doi: 10.1088/1361-6528/ac189f.

[4] J. Müller et al., "Ferroelectricity in Simple Binary ZrO2 and HfO2," Nano Lett, vol. 12, no. 8, pp. 4318–4323, Aug. 2012, doi: 10.1021/nl302049k.

[5] W. Zheng, K. H. Bowen, J. Li, I. Dabkowska, and M. Gutowski, "Electronic Structure Differences in ZrO2 vs HfO2," J Phys Chem A, vol. 109, no. 50, pp. 11521–11525, Dec. 2005, doi: 10.1021/jp053593e.

[6] P. D. Lomenzo, S. Slesazeck, T. Mikolajick, and U. Schroeder, "Thickness Scaling of AFE-RAM ZrO2 Capacitors with High Cycling Endurance and Low Process Temperature," in 2020 IEEE International Memory Workshop (IMW), IEEE, May 2020, pp. 1–4. doi: 10.1109/IMW48823.2020.9108146.

[7] P. D. Lomenzo, S. Li, L. Pintilie, C. M. Istrate, T. Mikolajick, and U. Schroeder, "Memory Window Enhancement in Antiferroelectric RAM by Hf Doping in ZrO2," IEEE Electron Device Letters, vol. 43, no. 9, pp. 1447–1450, Sep. 2022, doi: 10.1109/LED.2022.3189159.

[8] M. Pesic, U. Schroeder, S. Slesazeck, and T. Mikolajick, "Comparative Study of Reliability of Ferroelectric and Anti-Ferroelectric Memories," IEEE Transactions on Device and Materials Reliability, vol. 18, no. 2, pp. 154–162, Jun. 2018, doi: 10.1109/TDMR.2018.2829112.

[9] E. Kondratyuk and A. Chouprik, "Polarization Switching Kinetics in Thin Ferroelectric HZO Films," Nanomaterials, vol. 12, no. 23, p. 4126, Nov. 2022, doi: 10.3390/nano12234126.

[10] Y.-C. Chen, K.-Y. Hsiang, Y.-T. Tang, M.-H. Lee, and P. Su, "NLS based Modeling and Characterization of Switching Dynamics for Antiferroelectric/Ferroelectric Hafnium Zirconium Oxides," in 2021 IEEE International Electron Devices Meeting (IEDM), IEEE, Dec. 2021, pp. 15.4.1-15.4.4. doi: 10.1109/IEDM19574.2021.9720645.

[11] N. Gong, X. Sun, H. Jiang, K. S. Chang-Liao, Q. Xia, and T. P. Ma, "Nucleation limited switching (NLS) model for HfO2 -based metal-ferroelectric-metal (MFM) capacitors: Switching kinetics and retention characteristics," Appl Phys Lett, vol. 112, no. 26, p. 262903, Jun. 2018, doi: 10.1063/1.5010207.

[12] H. Dahlberg, A. E. O. Persson, R. Athle, and L.-E. Wernersson, "Ferroelectric-Antiferroelectric Transition of Hf1–xZrxO2 on Indium Arsenide with Enhanced Ferroelectric Characteristics for Hf0.2Zr0.8O2," ACS Appl Electron Mater, vol. 4, no. 12, pp. 6357–6363, Dec. 2022, doi: 10.1021/acsaelm.2c01483.

[13] H. Mulaosmanovic et al., "Novel ferroelectric FET based synapse for neuromorphic systems," in 2017 Symposium on VLSI Technology, IEEE, Jun. 2017, pp. T176–T177. doi: 10.23919/VLSIT.2017.7998165.

[14] J. Y. Jo, H. S. Han, J.-G. Yoon, T. K. Song, S.-H. Kim, and T. W. Noh, "Domain Switching Kinetics in Disordered Ferroelectric Thin Films," Phys Rev Lett, vol. 99, no. 26, p. 267602, Dec. 2007, doi: 10.1103/PhysRevLett.99.267602.

[15] H. Mulaosmanovic et al., "Switching Kinetics in Nanoscale Hafnium Oxide Based Ferroelectric Field-Effect Transistors," ACS Appl Mater Interfaces, vol. 9, no. 4, pp. 3792–3798, Feb. 2017, doi: 10.1021/acsami.6b13866.

[16] X. Lyu, M. Si, X. Sun, M. A. Capano, H. Wang, and P. D. Ye, "Ferroelectric and Anti-Ferroelectric Hafnium Zirconium Oxide: Scaling Limit, Switching Speed and Record High Polarization Density," in 2019 Symposium on VLSI Technology, IEEE, Jun. 2019, pp. T44–T45. doi: 10.23919/VLSIT.2019.8776548.